and plotting $\log \Sigma$ against $\log T$. It follows from Eq. (1) that these plots should be linear, with a slope equal to $-\alpha$, which provides a numerical method for calculating α directly from the data. The method is demonstrated in Fig. 3(a), where we plot experimental $\log \Sigma$ against $\log T$ for $Q = 0.38, 1.10, 2.09$, and 3.39 (symbols), and fit the linear dependence (solid lines) to the data in two discernible ranges ($T < T^*$ and $T > T^*$). These results confirm the conclusions drawn on the basis of $\log\sigma$ vs $T^{-\alpha}$ plots. For $T < T^*$, the hopping exponent is $\frac{1}{2}$ for two of these Q values (0.38 and 1.10), and $\frac{2}{5}$ for the other two ($Q = 2.09$ and 3.39). For $T > T^*$, the slopes of the linear fits have larger errors due this T range being smaller, but they are for all the samples close to -1, which is again in agreement with the notion that this regime corresponds to NNH. Furthermore, the crossover temperatures are here better defined than in Fig. 2, which allows us to determine them more accurately. The values of α, calculated from $\log \Sigma$ vs $\log T$ plots for all the samples, are shown in Fig. 3(b), and the corresponding values of $T^*(Q)$ are listed in Table I.

Hence, the σ characteristics of our differently doped samples have been analyzed using three independent methods which have given consistent results. First, $\log\sigma$ vs $T^{-\alpha}$ plots have been used to deduce the low-T values of α and the upper limit of the linear behavior. Second, $\alpha = 1$ has been fixed for these plots; the linearity has been confirmed on the high-T side and the low-T limit of this behavior has been identified. Third, the hopping exponents and crossovers between them have been addressed numerically by constructing and analyzing $\log \Sigma$ against $\log T$ plots. Having these results for α and $T^*(Q)$, we now turn to the inferences of our findings.

The fact that α assumes the values of $\frac{1}{2}$, $\frac{2}{5}$, and 1 implies the existence of Δ_C in our PANI-DBSA [25] because this is at the heart of the FTS model [26]. There is a question of whether one could extract Δ_C from our $\sigma(T)$ data, similarly as this was done from crossovers between different VRH regimes (different $\alpha < 1$) for HCl-doped PANI [32]. This method is based on addressing the energy range (symmetrical around E_F) containing states involved in the hopping transport, which is given by

$$\epsilon_\alpha = \alpha k_B T \left(\frac{T_\alpha}{T}\right)^\alpha \tag{3}$$

and plays the role of an activation energy [28]. The exponents $\alpha = \frac{2}{5}$ and $\frac{1}{2}$ reflect a reduction of the density of states for charge transport, originating in the opening of a linear or quadratic soft gap, respectively, for the energies E satisfying $|E - E_F| \leqslant \Delta_C$. When ϵ_α and Δ_C are of the same order, a crossover between $\alpha = \frac{1}{2}$ or $\frac{2}{5}$ (low T) and $\alpha = \frac{1}{4}$ or $\alpha = 1$ (high T) occurs at some T^* [41]. Hence, Δ_C can be estimated from

$$\Delta_C \approx \epsilon_\gamma(T^*) = \epsilon_\delta(T^*), \tag{4}$$

where γ and δ are hopping transport exponents below and above T^*, respectively. An elegant way to account for Eq. (4) directly from the data is to use that $\epsilon_\alpha = k_B T \Sigma(T)$ regardless of α, so Eq. (4) can be written as

$$\Delta_C \approx k_B T^* \Sigma(T^*), \tag{5}$$

which can be used to read Δ_C directly from experimental curves. The results of applying Eq. (5) to the data are plotted in Fig. 4 by triangles. On the other hand, by inserting $\delta = 1$ into Eq. (4), we obtain

$$\Delta_C \approx k_B T_1, \tag{6}$$

that is, Δ_C represents the activation potential of the NNH in our samples. This finding can also be supported by qualitative arguments, as follows. If energy restrictions for the hopping between nearest neighbors are marginal (we shall address this in more detail in Sec. III B), the potential an electron has to overcome in order to hop is the (screened) Coulomb interaction with the hole left behind, and this is what underlies the concept of Δ_C in a disordered system [28,42]. In Fig. 4,

TABLE I. Parameters extracted from experimental $\chi_p(T)$ for different Q: $n(E_F)$, N_C, $k_B^{-1}\Delta N_C/\Delta n(E_F)$, and $L_\parallel = \sqrt{\hbar^2 \Delta n(E_F)/8 m_e \Delta N_C}$. Ranges of linearity in $\chi_p(T)T$ are indicated, and T^* extracted from $\sigma(T)$ is also listed.

Q	T^* from $\sigma(T)$ (K)	T range of linear $\chi_p(T)T$ (K)	$n(E_F)$ [states(eV)$^{-1}$ (2 rings)$^{-1}$]	$N_C\ 10^{-3}$ [states (2 rings)$^{-1}$]	$k_B^{-1}\Delta N_C/\Delta n(E_F)$ (K)	$L_\parallel$ (Å)
3.39	146	10–170	4.24	19.03	152	8.50
	± 5	170–300	4.93	10.00		
2.92	196	10–190	3.99	21.02	193	7.56
	± 8	190–300	4.94	5.17		
2.60	208	10–200	3.22	26.64	204	7.38
	± 5	200–300	4.15	10.27		
2.09	213	10–200	2.29	33.63	201	7.43
	± 8	200–300	3.49	12.80		
2.06	213	10–190	2.97	29.32	197	7.48
	± 8	210–300	3.84	14.54		
1.10	219	10–200	3.84	26.77	211	7.23
	± 10	210–300	5.18	2.32		
0.38	221	10–220	0.53	11.83	232	6.88
	± 15	220–300	0.83	5.81		

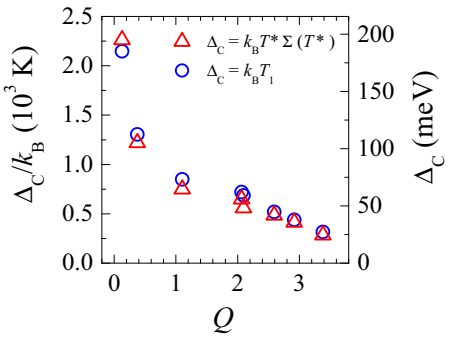

FIG. 4. Coulomb gap in PANI-DBSA, determined by two independent methods as explained in the text.

we plot by circles Δ_C extracted from the data according to Eq. (6), and these results show a good agreement with those from the application of Eq. (5). It can be seen in Fig. 4 that Δ_C decreases with increasing Q, dropping strongly from ~190 meV (2200 K) at $Q = 0.13$ to ~30 meV (350 K) at $Q = 3.38$. We believe that this appreciable decrease arises from an enhancement of the screening with increasing Q, which diminishes the disorder potential and reduces the corresponding Anderson localization.

B. Magnetic susceptibility and the onsite Coulomb interaction

The above analysis of $\sigma(T)$ provides valuable information but still leaves certain questions unanswered. While the decrease of Δ_C as Q grows implicates an enhancement of the screening and a consequent weakening of the disorder-induced localization, the reason for the crossover between VRH and NNH remains unclear when only these data are considered. In particular, an important part of the energy restrictions for the hopping between the localized states (which can be empty, singly or doubly occupied) is expected to originate in the onsite CEEI given by U (which opens a Hubbard gap). Since differently occupied sites carry different spin (0 or $\frac{1}{2}$), a natural way to approach this matter is to measure χ and compare these results to those for σ.

Measured $\chi(T)$ curves for different Q are shown in Fig. 5, where they are plotted as χT vs T (mole is defined per two rings, see Fig. 1). These plots are approximately linear, which implies [43–46]

$$\chi(T) = \frac{C_1}{T} + C_2 \,, \tag{7}$$

where C_1 and C_2 are independent of T. The first term on the right-hand side of Eq. (7) is the Curie susceptibility corresponding to localized spins at singly occupied protonation sites (see Fig. 1). The second term, C_2, comprises not only a strong diamagnetic component originating in atomic and ionic cores, but also a Pauli-type paramagnetic contribution of delocalized spins that hop from one localized state to another. Some of the curves exhibit cusps at temperatures of about 50 K, which is of little relevance for the current topic and has been discussed elsewhere [47,48]. When the diamagnetic contribution, which is of no importance for the behavior of localized and delocalized spins, is subtracted as explained in Ref. [30], one obtains the paramagnetic part χ_p of χ, as

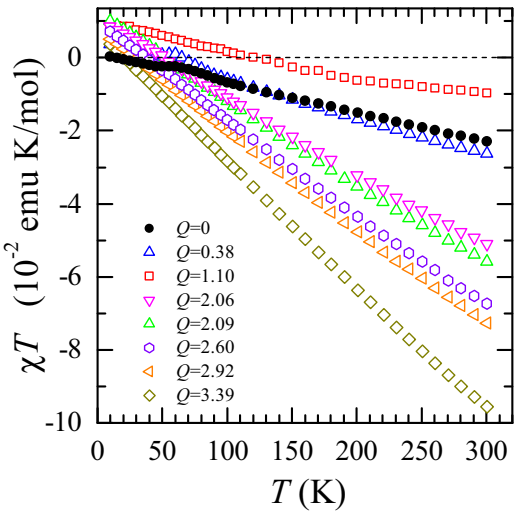

FIG. 5. χT vs T for different Q. Note that the intercept for the $Q = 0$ sample (black solid circles) is zero, i.e., there is no paramagnetism originating in localized spins.

we exemplify in Fig. 6 by plotting these data (symbols) for $Q = 0.38$, 1.10, 2.09, and 3.39. A closer inspection of these plots reveals that there are actually two ranges of linearity in $\chi_p T$ (indicated by the solid fit lines), with a crossover represented by a kink at a certain Q-dependent temperature T^* (marked by arrows). In Fig. 7, we plot this crossover temperature against Q by squares, and compare it to $T^*(Q)$ of

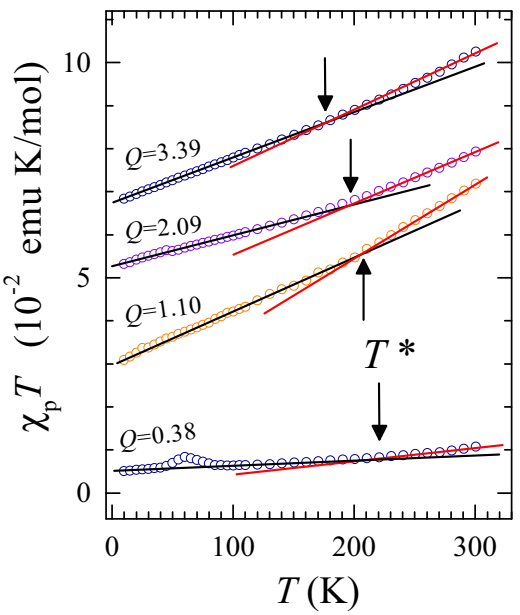

FIG. 6. Experimental $\chi_p T$ vs T (symbols) for $Q = 0.38$ and 1.10 (where $\alpha = \frac{1}{2}$ in VRH), and $Q = 2.09$ and 3.39 (where $\alpha = \frac{2}{5}$ in VRH). For clarity, the $Q > 0.38$ plots are offset vertically (each by 2 emuK/mol from the previous one). The arrows point to the positions of the crossover temperatures T^*, whereas the straight lines represent fits in the ranges of linearity. The cusp at $T \sim 50$ K for $Q = 0.38$ is of little relevance for the current topic and has been addressed elsewhere [47,48]. The physical parameters determining the linear fits are discussed in the text and listed in Table I.

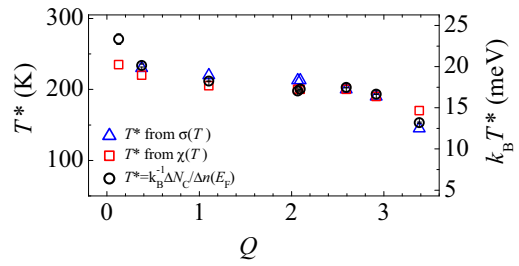

FIG. 7. Crossover temperature T^* as a function of Q, determined by three independent methods as explained in the text. Error bars are of the order of the symbol size.

the crossover between VRH and NNH, extracted from $\sigma(T)$ (triangles). Evidently, there is a good agreement between the crossover temperatures in $\sigma(T)$ and $\chi(T)$ over the whole Q range, which suggests the same underlying physics and justifies the use of the same symbol T^*. The circles represent T^* obtained by a third method, which is discussed later. A similar behavior was found for two HCl-doped PANI samples close to the full protonation [40], but these data were insufficient for establishing a more detailed physical picture. Less pronounced kinks in $\chi_p T$ vs T plots were also found for HCl-doped PANI at crossovers between different VRH mechanisms (i.e., different $\alpha < 1$), and the same mechanism, discussed below, underlies these crossovers as well (although they are less sharp than the crossover between VRH and NNH) [48].

From the plots demonstrated in Fig. 6, we can extract, separately for $T < T^*$ and $T > T^*$, several parameters which are useful in the subsequent discussion. Since the paramagnetic contribution of delocalized electrons is of a Pauli type, the slope C_2 is equal to $\mu_B^2 n(E_F)$, where μ_B is the Bohr magneton and $n(E_F)$ is an effective density of states of delocalized electrons around E_F. The intercept C_1 is equal to $N_C \mu_B^2/k_B$ because it corresponds to the Curie paramagnetism of localized spins $\frac{1}{2}$ (the concentration of which is N_C). In Table I, we list the calculated values of $n(E_F)$ and N_C for all Q. Other calculated quantities in Table I are $k_B^{-1}\Delta N_C/\Delta n(E_F)$ [where $\Delta n(E_F) = n(E_F; T > T^*) - n(E_F; T < T^*)$, and $\Delta N_C = N_C(T < T^*) - N_C(T > T^*)$], and the longitudinal localization length $L_\parallel$ (along the polymer chains).

One can note in Table I that there are two distinct regimes in $n(E_F)$: one for $Q \leqslant 1.10$ (where $\alpha = \frac{1}{2}$ in the VRH), and one for $Q > 1.10$ (where $\alpha = \frac{2}{5}$ in the VRH). In each of these regimes, $n(E_F)$ increases with increasing Q but $n(E_F)$ is for $Q = 1.10$ larger than that for $Q \approx 2$ although the conductivity is in the former case lower. However, we recall that these regimes differ in the structure of the Coulomb gap which is, as a function of energy, in the former case quadratic and in the latter case linear. This presumably affects the behavior of electrons close to E_F, which calls for a further modeling that is out of the main focus of this paper. On the other hand, the process at T^*, which is accounted for by $\Delta n(E_F)$ and ΔN_C, is insensitive to this difference, as follows. When the values of $k_B^{-1}\Delta N_C/\Delta n(E_F)$ from Table I are plotted on Fig. 7 (circles), it becomes clear that this quantity actually represents the same T^* obtained directly from the $\sigma(T)$ and $\chi_p(T)T$ curves. This leads to a conclusion that the thermal energy $k_B T^*$ plays a decisive role in the (de)localization of spins at the crossover between VRH and NNH. As T crosses T^* by heating up, Curie (localized) spins become delocalized, turning into Pauli spins, and the opposite happens in cooling down. Hence, N_C decreases (increases) by ΔN_C, whereas $n(E_F)$ simultaneously increases (decreases) by $\Delta n(E_F)$, the energy scale for this process being $k_B T^*$. For this to occur, the differences between electron energies associated with the occupancy of a localized state must be important for $T < T^*$ and marginal for $T > T^*$. We believe that a viable explanation for that can be found within the framework of the Kamimura model of χ_p for a system with the Anderson localization and onsite CEEI, which has been experimentally verified in a number of cases for doped semiconductors [33,34] and also applied to treat the coexistence of Curie-type and Pauli-type contributions in conducting disordered PANI with weak CEEIs [33,34]. In this model [33],

$$\chi_p = \frac{2\mu_B^2}{k_B T} \sum_j \left[2 + \exp\left(\frac{E_F - E_j - U_j}{k_B T} \right) + \exp\left(-\frac{E_F - E_j}{k_B T} \right) \right]^{-1} . \quad (8)$$

A hop of an electron to a singly occupied localized state costs an energy U; this sets restrictions in the sense that hopping to nearest neighbors is not necessarily the most favorable and the charge transport is consequently VRH. Simultaneously, the leading term in Eq. (8) is $\chi = N_S \mu_B^2/k_B T$, where N_S is the number of singly occupied states. This holds for any relation between U and the width W of the impurity band. When $W > U$ and T increases, the Curie contribution is suppressed and a Pauli-type behavior strengthens, becoming dominant at $T \sim U/k_B$. At $k_B T \gg U, W$, when electrons become nondegenerate (hot), a Curie-type $\chi_p(T)$ reappears but with a replacement of N_S by the total number of electrons; this regime is obviously not reached in our experiment.

In this picture, our samples are in the regime of $W > U$, and the crossover between the VRH and NNH occurs at $T^* \sim U/k_B$. The fulfillment of this criterion implies that $k_B T^*$ is large enough to diminish the energy restrictions for the hopping between differently occupied sites, which effectively closes the Hubbard gap and, in turn, sets NNH as the most efficient charge transfer mechanism. It can be seen in Fig. 7 that T^*, and consequently U, exhibits a weak decrease with increasing Q. If U were an on-atom SI, it should not depend on Q at all, but we recall that U is an on-mer SI, corresponding to more extended electron wave functions the tails of which overlap. This overlap is larger for less separated doped sites, i.e., larger Q, which increases the localization length and reduces U.

In order to test further the above picture of the effective closing of the Hubbard gap due to heating up, we have calculated the longitudinal localization length for the Anderson localization, given by [49,50]

$$L_{\parallel} \approx \sqrt{\frac{\hbar^2}{8 m_e U}}\,, \tag{9}$$

where m_e is the free-electron mass and U is in our calculation replaced by experimentally determined $k_B T^*$. As can be seen in Table I, the calculated $L_{\parallel}$ ranges from ~6.4 Å to ~8.5 Å (slightly increasing with increasing Q), which agrees well with the PANI mer size [35]. If we could estimate the localization length $L_{\perp}$ perpendicular to the polymer backbone, we would be able to calculate the localization volume $V_{loc} = L_{\perp}^2 L_{\parallel}$. We find it reasonable to assume that $L_{\perp} \sim 1$–2 Å, which is the width of the polymer backbone. This implies a relatively large V_{loc} which is by a factor of $L_{\parallel}/L_{\perp} \sim 5$ larger than that typical of a localization on a single atom. An implication of this assessment is that thermal activation within disorder band in doped PANI gives rise to a relatively high σ because $T_{\alpha} \propto 1/V_{loc}$ [5].

IV. CONCLUSIONS

Polyaniline (PANI) doped with dodecylbenzenesulfonic acid (DBSA) shares many properties with other variants of doped (electrically conducting) PANI, such as a protonation mechanism which leads to the injection of conducting charge and a relatively high conductivity, a strongly disordered structure of entangled polymer chains that results in the Anderson localization, an electrical transport via charge hopping from one localized state to another, etc. On the other hand, PANI-DBSA exhibits a behavior which is seldom found not only in doped PANI, but also in conducting polymers generally: it undergoes a crossover from a low-T variable range hopping (VRH) to a high-T nearest-neighbor hopping (NNH) below room temperature and over a wide doping range. This property was useful in an experimental confirmation [25] of the Fogler-Teber-Shklovskii model [26] of hopping transport in three-dimensional networks of chain conductors, implying the presence of a long-range Coulomb interaction that opens a soft Coulomb gap Δ_C within the impurity band. However, PANI-DBSA is a system with a short-range, onsite Coulomb interaction U as well, which generally may lead to the Mott localization. Namely, the protonation of PANI leads to singly occupied localized states, each carrying a spin $\frac{1}{2}$, which may also become empty or doubly occupied as the charge hops, and in this process, the onsite Coulomb repulsion cannot be disregarded. Having the above in mind, we here address the coexistence of long- and short-range Coulomb interactions in Anderson-Mott insulators.

Our investigation is based on comparative measurements and analysis of the T dependencies of the electrical conductivity σ and magnetic susceptibility χ of own-made PANI-DBSA pellets. The doping range of our samples covers room-temperature conductivity between 10^{-10} and 10^{3} S/m, i.e., we have tackled the physics outlined above from a virtually nonconducting to a relatively well-conducting state of a same material. The shapes of $\sigma(T)$ and $\chi(T)$ are characteristic of doped PANI, that is, $\sigma(T)$ contains a signature of a thermally activated hopping transport, whereas the paramagnetic part of $\chi(T)$ is a sum of a $1/T$ Curie-type and a T-independent Pauli-type contribution. By analyzing the $\chi(T)$ curves, we have found that they also exhibit a crossover from a low-T to a high-T regime, and that the crossover temperature T^* is, over the whole doping range, the same as that of the VRH-NNH crossover in $\sigma(T)$. Using the Kamimura model for the $\chi(T)$ of a system with the Anderson localization and a finite U, we conclude that the VRH-NNH crossover at T^* occurs because the thermal energy $k_B T^*$ is of the order of the energy differences between differently occupied localized states. Hence, in this picture, $U \sim k_B T^*$. Using this assumption, we calculate the longitudinal electron localization length $L_{\parallel}$ and obtain that it is basically equal to the PANI-DBSA mer size. This result is consistent with the structure of PANI-DBSA polymer chains and explains why U is much smaller than in the case of localized states on single atoms. In addition to $L_{\parallel}$, we determine several other parameters of importance, these being Δ_C, the effective density of states of delocalized electrons around the Fermi energy, and the density of localized Curie spins.

We find that Δ_C is robust but strongly doping dependent, ranging from 30 meV (350 K) to 190 meV (2200 K) at the highest and lowest doping, respectively, and it plays the role of the activation energy in the NNH. The strong reduction of Δ_C by doping is attributed to an enhancement of the screening of the long-range Coulomb interaction as the density of delocalized charge grows. In contrast, U is much smaller and decreases with increasing doping from 20 meV (230 K) to 12 meV (145 K). For an on-atom electron-electron interaction, U would be independent of doping, but U is here an on-mer interaction and its doping dependence is a consequence of a larger overlapping of the localized electron wave functions when these are less separated.

A small Hubbard gap U that is situated within a larger Coulomb gap Δ_C is the main feature of our system, and these two gaps govern the spin and charge dynamics in PANI-DBSA. The property of having a gap within a gap appears in many different systems, e.g., underdoped cuprate superconductors, Bechgaard salts with spin-density-wave order, etc., where a small gap or pseudogap is usually within a large hard Hubbard gap [51,52]. In our system, in contrast, the Hubbard gap is the smaller one of the two coexisting gaps. Yet, such an attenuation of the Hubbard gap (which is in our system due to an on-mer localization) is not surprising when relevant electron wave functions are spread over several sites/atoms. Because U is small, Δ_C represents the dominant energy scale in PANI-DBSA since the screening of the long-range Coulomb interaction is only partial due to the presence of disorder in the system.

ACKNOWLEDGMENTS

Discussions with L. Forró, S. Teber, I. Kupčić, and B. Batlogg are gratefully acknowledged. This work has been supported by Croatian Science Foundation under the Project No. 6216.

[1] P. W. Anderson, Phys. Rev. **109**, 1492 (1958).
[2] A. Lagendijk, B. van Tiggelen, and D. S. Wiersma, Phys. Today **62**(8), 24 (2009).
[3] N. F. Mott, Proc. Phys. Soc. London, Sect. A **62**, 416 (1949).
[4] J. Hubbard, Proc. R. Soc. London, Ser. A **276**, 238 (1963).
[5] N. F. Mott, *Metal-Insulator Transitions*, 2nd ed. (Taylor & Francis, London, 1990).
[6] P. A. Lee and T. V. Ramakrishnan, Rev. Mod. Phys. **57**, 287 (1985).
[7] M. Imada, A. Fujimori, and Y. Tokura, Rev. Mod. Phys. **70**, 1039 (1998).
[8] J. H. Davies, J. Phys. C: Solid State Phys. **17**, 3031 (1984).
[9] H. von Löhneysen, Ann. Phys. (Berlin) **523**, 599 (2011).
[10] *Conductor-Insulator Quantum Phase Transitions*, edited by V. Dobrosavljević, N. Trivedi, and J. M. Valles, Jr. (Oxford University Press, Oxford, 2012).
[11] S. Teber, Eur. Phys. J. B **49**, 289 (2006).
[12] D. Belitz and T. R. Kirkpatrick, Rev. Mod. Phys. **66**, 261 (1994).
[13] A. Richardella, P. Roushan, S. Mack, B. Zhou, D. A. Huse, D. D. Awschalom, and A. Yazdani, Science **327**, 665 (2010).
[14] E. Prati, M. Hori, F. Guagliardo, G. Ferrari, and T. Shinada, Nat. Nanotechnol. **7**, 443 (2012).
[15] K. Byczuk, W. Hofstetter, and D. Vollhardt, Int. J. Mod. Phys. B **24**, 1727 (2010).
[16] D. M. Basko, I. L. Aleiner, and B. L. Altshuler, Ann. Phys. (NY) **321**, 1126 (2006).
[17] I. S. Burmistrov, I. V. Gornyi, and A. D. Mirlin, Phys. Rev. Lett. **108**, 017002 (2012).
[18] G. Tzamalis, N. A. Zaidi, C. C. Homes, and A. P. Monkman, Phys. Rev. B **66**, 085202 (2002).
[19] M. Schreiber, S. S. Hodgman, P. Bordia, H. P. Lüschen, M. H. Fischer, R. Vosk, E. Altman, U. Schneider, and I. Bloch, Science **349**, 842 (2015).
[20] A. Aspect and M. Inguscio, Phys. Today **62**(8), 30 (2009).
[21] G. Roati, C. D'Errico, L. Fallani, M. Fattori, C. Fort, M. Zaccanti, G. Modugno, M. Modugno, and M. Inguscio, Nature (London) **453**, 895 (2008).
[22] M. Lewenstein, A. Sanpera, V. Ahufinger, B. Damski, A. Sen(De), and U. Sen, Adv. Phys. **56**, 243 (2007).
[23] B. Deissler, M. Zaccanti, G. Roati, C. D'Errico, M. Fattori, M. Modugno, G. Modugno, and M. Inguscio, Nat. Phys. **6**, 354 (2010).
[24] H. von Löhneysen, Disorder, electron-electron interactions and the metal-insulator transition in heavily doped Si:P, in *Advances in Solid State Physics 40*, edited by B. Kramer (Springer, Berlin, 2000), pp. 143–167.
[25] M. Baćani, M. Novak, I. Kokanović, and D. Babić, Synth. Met. **172**, 28 (2013).
[26] M. M. Fogler, S. Teber, and B. I. Shklovskii, Phys. Rev. B **69**, 035413 (2004).
[27] R. Menon, C. O. Yoon, D. Moses, and A. J. Heeger, Metal-insulator transition in doped conducting polymers, in *Handbook of Conducting Polymers*, edited by T. A. Skotheim, R. L. Elsenbaumer, and J. R. Reynolds, 2nd ed. (Marcel Dekker, New York, 1998), pp. 27–84.
[28] B. I. Shklovskii and A. L. Efros, *Electronic Properties of Doped Semiconductors* (Springer, Berlin, 1984).
[29] A. L. Efros and B. I. Shklovskii, J. Phys. C: Solid State Phys. **8**, L49 (1975).
[30] M. Baćani, D. Babić, M. Novak, I. Kokanović, and S. Fazinić, Synth. Met. **159**, 2584 (2009).
[31] S. Stafström, J. L. Brédas, A. J. Epstein, H. S. Woo, D. B. Tanner, W. S. Huang, and A. G. MacDiarmid, Phys. Rev. Lett. **59**, 1464 (1987), and references therein.
[32] M. Novak, I. Kokanović, D. Babić, M. Baćani, and A. Tonejc, Synth. Met. **159**, 649 (2009).
[33] H. Kamimura, Electron-electron interactions in the Anderson-localised regime near the metal-insulator transition, in *Electron-Electron Interactions in Disordered Systems*, edited by A. L. Efros and M. Polak (North Holland, Amsterdam, 1985), pp. 555–617.
[34] H. Kamimura and H. Aoki, *The Physics of Interacting Electrons in Disordered Systems* (Clarendon, Oxford, 1990).
[35] J. P. Pouget, M. E. Jozefowicz, A. J. Epstein, X. Tang, and A. G. MacDiarmid, Macromolecules **24**, 779 (1991).
[36] M. McElfresh, *Fundamentals of Magnetism and Magnetic Measurements - Featuring Quantum Design's Magnetic Property Measurement System* (Quantum Design, San Diego, 1994).
[37] A. G. MacDiarmid, J.-C. Chiang, A. F. Richter, and A. J. Epstein, Synth. Met. **18**, 285 (1987).
[38] A. G. MacDiarmid, Rev. Mod. Phys. **73**, 701 (2001).
[39] Additionally, DBSA is a surfactant leading to technologically important solubility in common solvents such as chloroform, which is rare within the whole class of doped PANI.
[40] M. Novak, I. Kokanović, D. Babić, and M. Baćani, J. Non-Cryst. Solids **356**, 1725 (2010).
[41] $\alpha = \frac{1}{4}$ has been in our PANI-DBSA observed only for the highest doping of $Q = 3.39$ (and in a rather narrow T range of $\sim$35K below the eventual appearance of $\alpha = 1$) (see Ref. [25] for details). This peculiarity has a marginal effect on the results for Δ_C presented in Fig. 4.
[42] A. L. Efros, B. Skinner, and B. I. Shklovskii, Phys. Rev. B **84**, 064204 (2011).
[43] V. I. Krinichnyi, Appl. Phys. Rev. **1**, 021305 (2014).
[44] P. Phillips, Phys. Rev. B **49**, 4303 (1994).
[45] N. S. Sariciftci, A. J. Heeger, and Y. Cao, Phys. Rev. B **49**, 5988 (1994).
[46] D. Chaudhuri, A. Kumar, R. Nirmala, D. D. Sarma, M. García-Hernández, L. S. Sharath Chandra, and V. Ganesan, Phys. Rev. B **73**, 075205 (2006).
[47] M. Baćani, Ph.D. thesis, University of Zagreb, 2014.
[48] M. Novak, I. Kokanović, M. Baćani, and D. Babić, Eur. Phys. J. B **83**, 57 (2011).
[49] N. J. Pinto, P. K. Kahol, B. J. McCormick, N. S. Dalal, and H. Wan, Phys. Rev. B **49**, 13983 (1994).
[50] N. F. Mott and E. A. Davis, *Electronic Processes in Non-Crystalline Materials*, 2nd ed. (Clarendon, Oxford, 1979).
[51] *Handbook of High-Temperature Superconductivity*, edited by J. R. Schrieffer and J. S. Brooks (Springer, New York, 2007).
[52] M. Dressel, A. Schwartz, G. Grüner, and L. Degiorgi, Phys. Rev. Lett. **77**, 398 (1996).